Polymer 51 (2010) 1796–1804

Contents lists available at ScienceDirect

Polymer

journal homepage: www.elsevier.com/locate/polymer

Structure & strength of silica-PDMS nanocomposites

Adrian Camenzind [a,1], Thomas Schweizer [b], Michael Sztucki [c], Sotiris E. Pratsinis [a,*]

[a] Particle Technology Laboratory, Institute of Process Engineering, Department of Mechanical and Process Engineering, ETH Zurich, Sonneggstrasse 3, CH-8092 Zurich, Switzerland
[b] Institute of Polymers, Department of Materials, ETH Zurich, Wolfgang-Pauli-Strasse 10, CH-8093 Zurich, Switzerland
[c] European Synchrotron Radiation Facility (ESRF), BP 220, F-38043 Grenoble Cedex, France

ARTICLE INFO

Article history:
Received 16 September 2009
Received in revised form
7 February 2010
Accepted 18 February 2010
Available online 23 February 2010

Keywords:
Reinforcing
Immobilized Polymer
Fractal

ABSTRACT

Silica nanoparticles having specific surface area (*SSA*) 50–300 $m^2\ g^{-1}$ were admixed into vinyl-terminated dimethylsiloxy monomer with a dual asymmetric centrifuge (planetary mixer) and cured to form PDMS-based nanocomposites containing up to 12 vol% SiO_2. Thin sections of cured nanocomposites obtained by a cryostate-microtome were analyzed by TEM while small and ultra small angle X-ray scattering (U/SAXS) was used to determine nanocomposite structure: filler primary particle, aggregate (chemically or sinter-bonded particles) and agglomerate (physically-bonded particles) size as a function of mixing duration and filler concentration. More aggregated silicas with higher *SSA* exhibited denser crosslinking than less aggregated ones regardless of crosslinker content as determined by swelling nanocomposites in toluene at equal filler content. The nanocomposite strength was determined by tensile tests (Young's modulus and elongation at break). Consistent with "bound rubber" theory, the Young's modulus of the nanocomposites increased non-linearly with increasing filler volume fraction.

1. Introduction

The reinforcing potential of admixing particles in polymers was recognized first in the rubber industry where carbon black filled vulcanizates were made from natural rubber [1]. Active particles interact with the polymer matrix by adsorption of polymer molecules at their surface (immobilization) and with each other [1]. Similarly, reinforcing with nanostructured SiO_2 particles is applied to polyethylene or polydimethylsiloxane (PDMS) as these polymers have relatively low mechanical strength [1].

The reinforcement of PDMS by hydrophilic SiO_2 is attributed to particle–particle or particle-polymer interactions. During particle–particle interactions, hydrogen bonding between particles significantly increases the resistance to the applied force [2]. Bonding strength and resistance are weakened [3] by altering the particles from hydrophilic to hydrophobic through passivation of their surface silanol groups (–OH) by chlorosilanes [4–6], methoxysilanes [4] or silazanes [5–7]. Strong particle-polymer interactions take place when polymer molecules bond to surface silanol groups forming a thin layer of "bound rubber" [8], 1–5 nm thick, depending on polymer molecular weight or chain length [2,9]. The reinforcement depends on adhesion forces (polymer-particle), particle concentration and their specific surface area as well as polymer molecular weight [9,10]. Moreover, passivating silanol groups at the particle surface decreases particle-polymer interactions, "bound rubber" thickness [9] and viscosity during processing, an important feature for the compounding industry [6].

Addition of other nanostructured materials like TiO_2 or ZrO_2 for improved resistance to degradation by heat and Al_2O_3 for improved thermal conductivity, abrasion resistance and flame retardancy [11] has widened the applications for PDMS-based nanocomposites. Today flame aerosol technology is used for large-scale manufacture of such filler particles at several tons/hour [12]. Recently, an array of nanoscaled, sophisticated products such as catalysts, sensors, dental and bone replacement composites, phosphors, fuel cell and battery materials, and even nutritional supplements have been made in flames [13]. Blending, however, such sophisticated particles into polymers and evaluating the effect of particle size, morphology and composition on nanocomposite performance is challenging. For example, making dental Ta_2O_5/SiO_2 composites required different procedures [14] and materials than pure silica. Most often, reinforcing particles are mechanically blended into PDMS polymers prior to curing of the composite (in-situ polymerization) despite known drawbacks as time- and energy-consumption as well as loss of control on the degree of particle dispersion that leads to large agglomerates [1].

* Corresponding author. Tel.: +41 44 632 31 80; fax: +41 44 632 15 95.
E-mail address: pratsinis@ptl.mavt.ethz.ch (S.E. Pratsinis).
[1] Present address: Optotune AG, Ueberlandstrasse 129, CH-8600 Dübendorf, Switzerland.

0032-3861/$ – see front matter © 2010 Elsevier Ltd. All rights reserved.
doi:10.1016/j.polymer.2010.02.030

Most lab scale mixers for highly viscous media [15] (Banbury™ or Brabender™ mixer [16], kneeder [2,3,6,7], single or double screw extruder) have a batch volume of about 1 L while extruder operate continuously, in contrast. With particle loadings up to 30 vol%, however, there is a need for mixers with smaller mixing volumes to make nanocomposite screening feasible. A blender which can be operated at low mixing volumes (1–100 ml) is the so-called dual asymmetric centrifuge (DAC) or planetary mixer [17]. This is used for processing of polymeric blends based on epoxy resins [18] or PDMS [19,20] or particle-polymer composites with hydrophilic or hydrophobic SiO_2 [21] for dental composites [22], electronic applications [23] and conductive particles in PDMS [24]. The DAC has been applied also for admixing food additives [25], carbon nanotubes in epoxy resins [26] or anti-fouling particles in PDMS [27]. However, little is known about the effect of mixing conditions on particle dispersion and nanocomposite performance.

The goal of this paper is to understand the reinforcing of PDMS-based nanocomposites by commercially available, more (e.g. Aerosil 150, 200, 300) or less aggregated (e.g. OX50) SiO_2 fillers through detailed investigation of filler structure in nanocomposites by non-intrusive small and ultra small angle X-ray scattering. These measurements are compared to nitrogen adsorption data (BET) for primary particle size, and microscopic (TEM) images of nanocomposites at various SiO_2 loadings. The swelling ability of cured samples is investigated to determine the optimum crosslinker concentration. The mechanical strength of such composites is measured as a function of component mixing duration and compared to structural characteristics of the fillers. Mechanical properties of these nanocomposites are analyzed focusing on their Young's modulus and elongation at break from tensile strength measurements. Finally, the potential of classic "bound rubber" theory, originally developed for carbon black filled rubbers [28], is explored here for describing the strength of silica/PDMS nanocomposites.

2. Experimental

2.1. Materials

Commercially available, hydrophilic fumed SiO_2 nanoparticles most (Aerosil A150, A200 and A300, Evonik, formerly Degussa) or less aggregated (Aerosil OX50, Evonik) were used as received. Their specific surface area (*SSA*, $m^2\ g^{-1}$) was determined by N_2 (PanGas, $>$ 99.9999%) adsorption at −196 °C (Micromeritics, Tristar 3000) [29]. The samples were degassed (N_2) at 150 °C for 1 h prior to analysis. Measured *SSA* corresponded to that given by the manufacturer (in brackets): OX50: 43 (50 ± 15), A150: 129 (150 ± 15), A200: 192 (200 ± 25) and A300: 269 (300 ± 30) $m^2\ g^{-1}$, respectively.

For polydimethylsiloxane (PDMS) based nanocomposites, a vinyl-terminated dimethylsiloxy monomer (DMS-V31, number-average molecular weight M_n = 28,000, η = 970 mPa s, 0.18–0.26 wt.% vinyl, ρ = 0.97 g cm^{-3}, ABCR, Germany) was cured with polymethylhydrosiloxane (PMHS, M_n = 1700–3200, η = 15–40 mPa s, ρ = 1.004 g cm^{-3}, Aldrich) as crosslinker [30]. A catalyst (platinum carbonyl cyclovinyl-methyl-siloxane complex, 1.85–2.1 wt.% Pt in vinyl-methylcyclosiloxane, ABCR) was used for curing the above monomer. No additional crosslinking inhibitor to prevent premature curing (applied in commercially available (addition) cure systems), was used [17].

2.2. Nanocomposite preparation

Monomer and SiO_2 particles (volume fraction, ϕ_v, up to 12 vol%) were mixed in a DAC (FlackTek SpeedMixer™ 150 FVZ, Hauschild, Germany) [17] at 10 cm^3 batches in a standard polypropylene 25 cm^3 screw cap vessel. The molar ratio of crosslinker (PMHS) and monomer was 10–30 mol% depending on the optimum concentration for sufficient crosslinking [30]. Monomer and catalyst (15 ppm Pt of the sample weight) were mixed at 3000 rpm for 2 min (t_{mix}) with a speed ramp of 1000 rpm s^{-1}. Particles were then added in 1–3 equal doses depending on type and amount [23]. Each particle dose was admixed at 3000 rpm for 15 s (after reaching it at 200 rpm s^{-1}). In-between dosing, particles adhering to the walls were manually replaced back into the composite mixture. This was followed by mixing at 3000 rpm (after reaching it at 1000 rpm s^{-1}) for t_{mix} = 10–40 min.

The DAC cap containing the particle/monomer/catalyst suspension was cooled with water (10 °C) for 5 min prior to adding the crosslinker (PMHS). Admixing of crosslinker was then performed at 3000 rpm for 1 min after reaching it with 50 rpm s^{-1}. Here, two components with a significant viscosity difference were mixed. Gentle initial mixing at a slow speed ramp prevents splashing the low viscosity PMHS to the vessel wall. Applying faster speed ramps resulted in inhomogeneously mixed components, as prolonged mixing at high speed result in elevated temperatures which leads to premature curing. High particle concentrations increase dramatically the suspension viscosity and prevent efficient DAC operation. For non-modified, hydrophilic silica particles that exhibit strong particle-polymer interactions [5], the maximum particle loadings are about 12 vol% for OX50 and 7 vol% for A150, A200 or A300 [23]. This was confirmed visually by adding few mg of red colorant Fe_2O_3 particles (Bender & Hobein AG, Switzerland) instead of crosslinker and following the above procedure for crosslinker admixing.

These as-prepared nanocomposites were cured in a 2-piece hardened stainless steel mold (Hertsch & Cie, 1.2316, hardened at 500 °C for 2 h prior to use) to form 1 mm thick, bubble-free composite disks (70 mm diameter) at 90 °C for 90 min in a ventilated oven (Memmert, ULE 500). In the center of these disks, a thinner section, 10 mm in diameter and approximately 200 μm thick, is formed that is used for U/SAXS characterization.

2.3. Nanocomposite characterization

2.3.1. Mechanical properties: swelling ability and tensile strength

To determine the optimum crosslinker concentration, cured nanocomposites were swelled in toluene [31]. For all composites a mixing duration of 40 min was applied. Circular composite samples (diameter 12 mm) were cut out and their initial weight, m_i, was measured (Mettler Toledo, AB135-S/FACT, accuracy: ±0.03 mg). Swelling them in toluene (Riedel-de Haën, purity ≥ 99%) for 24 h increased their weight, m_w, followed by drying (vacuum dryer VC20, Salvis Lab, Switzerland) at 80 °C and 30 mbar for 24 h that resulted in their dry mass, m_d. The reduction of weight is attributed to washing out of non-crosslinked compounds [31]. The sample absorbency $A = (m_w - m_d)/m_d$ was measured [31] which is inversely proportional to crosslinking density [32] or composite strength.

From the cured nanocomposites, dumb-bell shaped samples were punched out following DIN53504 (test region: sample width b = 2 mm, gauge length L_0 = 10 mm) with a stainless steel punch. Tensile measurements were done with an Instron (Model 5864) at 200% strain min^{-1} at room temperature and an average standard deviation of 4 samples is reported here. Composite thickness, a (≈1 mm) of each specimen was measured with a digital dial gauge (Mitutoyo, Absolute, ID-C112CB, 0.4–0.7 N, mounted with a flat insert steel, diameter 5 mm, accuracy: ± 3 μm) to determine the undeformed cross-sectional area, $S = b \times a$. The engineering (or nominal) stress, $\sigma = F/S$ (with F being the measured force), was plotted against the engineering strain, $\epsilon = \Delta L/L_0$ (wherein $\Delta L = L - L_0$ with L being the apparent gauge length) following DIN53504. The Young's modulus E was determined within $\epsilon \leq 0.05$ and is

calculated from the straight line portion [6] of σ versus ϵ as $\epsilon \to 0$. The elongation at break is $\epsilon_b = L_b/L_0$, where L_b is the maximum gauge length before break.

2.3.2. Particle structure and dispersion: TEM imaging and X-ray scattering

For visualization of the particle dispersion in the composite, a cryostate-microtome (Ultracut S + cryo-FCS, Reichert-Leica) was used. Test samples ($1 \times 1 \times 2$ mm^3) were mounted onto a copper sample holder and cooled with liquid N_2 down to -120 °C. The cutting speed was set to 0.4 mm s^{-1} (step depth 70 nm) and thin sections were cut with a diamond knife (cryo 35°, DiATOME, Switzerland) at 41° cut angle [33]. The resulting thin sections were picked with a perfect loop dipped into sucrose (2.2 mol l^{-1} in deionized water). The sucrose immediately freezes once placed into the cooled section of the cryo-microtome. The thin composite section was then collected by touching it (the frozen sucrose) with the perfect loop. At room temperature the sucrose melts forming a liquid drop that contains the thin composite section. A transmission electron microscopy (TEM) grid (hexagonal copper grid, 200 mesh, Plano, Germany) can then be collected with the perfect loop on which the sucrose and thin composite section was attached above and can than be placed into deionized water. The TEM grid floats on the water surface and the sucrose is dissolving into the water for 5 min while the composite section stays on the TEM grid (and the composite section attached to it) is collected and dried at room temperature. Subsequent TEM analysis was performed on a CM30 microscope (FEI; LaB6 cathode, operated at 300 kV) and images were recorded on a slow-scan CCD camera.

To determine filler particle characteristics in the nanocomposites two complementary X-ray scattering techniques were used at the European Synchrotron Radiation Facility (ESRF, high brilliance beam line ID02, Grenoble, France) [29]. First, the primary particles and their aggregates were characterized simultaneously using a pinhole SAXS setup [34]; and second, larger scattering objects (agglomerates), 0.05–1 μm, were characterized by a Bonse–Hart ultra small-angle X-ray scattering (USAXS) camera [35,36]. A highly collimated monochromatic X-ray beam ($\lambda = 1$ Å) with a cross-sectional area of 200×200 μm^2 was used for SAXS. The beam was directed to the thinnest section of the nanocomposite disk. The scattered intensity was recorded by a fiber optically coupled CCD (charge coupled device) based X-ray detector (FReLoN) housed in an evacuated flight tube. The sample to detector distance was 10 m and typical acquisition time ranged from 0.1 to 1 s for highly concentrated composites (11.7 vol%) and particle-free polymers, respectively. SAXS and USAXS patterns were normalized to an absolute scale (taking into account the sample thickness, Table 1), azimuthally averaged and background subtracted (using particle-free polymers) to obtain the scattered intensity $I(q)$ as a function of scattering vector, $q = 4\pi sin(\theta/2)/\lambda$, with θ being the scattering angle [37], for $q = 0.001$–0.05 Å^{-1}. The Bonse–Hart USAXS camera allowed detection over a wider q-range, especially at low q (10^{-4}–0.02 Å^{-1}). The recorded intensity profiles were normalized to an absolute scale using the peak intensity and the known acceptance angle defined by the analyzer crystals. However, with the USAXS camera longer measurement times (~5 min) were required.

Particle characteristics were determined from combined U/SAXS scattering spectra (10^{-4}–0.05 Å^{-1}) following the unified fit model [37,38]: aggregate and agglomerate radii of gyration (R_{g2}, R_{g3}), aggregate mass fractal dimension (D_f), primary particle diameter ($d_{v/s}$) [38,39], number of primary particles per aggregate (n) and silica volume fraction (ϕ_v). In addition, to composites, polymer-free particle characteristics were obtained from dry powders placed between two adhesive tapes (Scotch, Magic, 3M) [40]. Particle-free adhesive tapes were used for background subtraction.

3. Theory

Einstein [41] proposed a linear expression for particle reinforcement (ratio of suspension viscosity over that of pure solvent, hence a relative viscosity) as function of ϕ_v at rather low particle concentrations (<1 vol%). This has been extended analytically and empirically to describe the rather exponential increase of suspension viscosity at higher particle concentrations [42,43]. In particle-filled viscoelastic suspensions, however, reinforcing does not scale with ϕ_v but with the so-called effective volume fraction, $\phi_{v,\mathrm{eff}}$, which accounts for the increase in volume by attachment of polymer chains to the particle surface [44]. A linear relation of $\phi_{v,\mathrm{eff}} = \beta \times \phi_v$ has been proposed where β is the "effectiveness factor" describing the capacity of a particle to immobilize polymer chains [28]. Lately, a description of β as a function of primary particle size, d_p, mean number of adjacent particles, c_N, the so-called coordination number [45] and "bound rubber" thickness, h, has been proposed [44]. So the ratio of effective particle volume (including "bound rubber") to the nominal particle volume, V_p, is:

$$\beta = \frac{V_p + V_{br} - c_N \cdot \Delta V}{V_p} = 1 + \frac{V_{br}}{V_p} - c_N \cdot \frac{\Delta V}{V_p}$$
$$= 1 + 6\frac{h}{d_p} + 12\left(\frac{h}{d_p}\right)^2 + 8\left(\frac{h}{d_p}\right)^3 - c_N\left[3\left(\frac{h}{d_p}\right)^2 + 4\left(\frac{h}{d_p}\right)^3\right] \quad (1)$$

where V_{br} is the immobilized polymer ("bound rubber") on a single non-aggregated or agglomerated particle (having no contact to adjacent particles). For aggregated particles a correction term for the interpenetrating "bound rubber" layer (ΔV) of adjacent particles in an aggregate is used [44]. The reinforcing of carbon black and SiO_2 in natural rubber blends using Eq. (1) was in good agreement with data [44] for $h = 5.7$ nm and $c_N = 3.3$ that resulted in an effectiveness factor, β, 4.26 for A300 and 1.77 for OX50 SiO_2 evaluated up to $\phi_v = 10$ vol%.

4. Results and discussion

4.1. Particle structure and dispersion in cured nanocomposites

Fig. 1 shows TEM images of thin sections (100–200 nm thick) of silica (OX50 and A300) filled composites. Low magnification images (a, c, e) show the broad distribution of filler particles in the composites while enlarged ones (b, d, f) show finer detail of the individual particles. Fig. 1a–d shows sections of 6.2 vol% A300 filled composites mixed for 10 (a, b) and 30 min (c, d). Fig. 1c shows apparently less SiO_2 than Fig. 1a even though both contain identical particle loadings. This might be misleading as it is rather difficult to precisely control the composite section thickness [33] and avoid strain on the composite sections while unfreezing during microtome thin sectioning. Moreover, TEM images only show small sample fractions that are hardly representative. Agglomerates or aggregates in Fig. 1a,b are in the order of several hundred of nanometers. For 10 min of mixing, particle structures larger than 1 μm were observed. In contrast, mixing for 30 min results in smaller ones. Fig. 1e,f depicts a 11.7 vol% OX50 filled composite mixed for 30 min. Agglomerates in the order of ≥0.5 μm are detected while the distinction of aggregates from agglomerates by these images is not possible.

Far more insightful information can be obtained by techniques averaging information over a much bigger fraction of the nanocomposites reducing the risk of being misled when relying on TEM alone as above. Fig. 2 shows the combined ultra small (USAXS) and small angle X-ray scattering (SAXS) as a function of the scattering vector q of nanocomposites filled with 6.2 vol% (a) OX50 and (b)

Table 1
Particle characteristics by small angle X-ray scattering (SAXS) of composites made by mixing for 10–40 min and curing PDMS with fumed silica of 11.7 vol% or 6.2 vol% OX50 and 6.2 vol% A150, A200 and A300. BET equivalent primary particle size (d_{BET}) and nominal particle loading (ϕ_v), are compared to $d_{v/s}$ and SiO_2 solid volume fraction obtained from SAXS.

Particle	sample thickness, μm	Mixing duration, min t_{mix}	SiO_2 volume fraction, ϕ_v, vol%		Primary particle size			Aggregate			Agglomerate
					d_{BET}, nm	$d_{v/s}$, nm		Mass fractal dimension D_f	size, $2\cdot R_{g2}$, nm d_g	Number of primary particles n	size, $2\cdot R_{g3}$, nm d_l
			nominal	SAXS		dry	composite				
OX50	211	10	11.7	13.4	55	41.5	43.3	1.74	244	6.5	513
	210	20		13.2			42.8	1.74	236	6.0	647
	213	30		12.7			42.6	1.74	236	6.4	746
	212	40		13.8			43.3	1.75	251	6.3	494
	211	10	6.2	6.7			40.5	1.75	270	4.8	>1 μm
	212	20		6.6			40.9	1.75	269	4.8	
	211	30		6.6			40.8	1.75	270	4.8	
	209	40		6.5			40.5	1.75	281	4.6	
A150	211	10	6.2	7.6	18	15.4	15.3	1.84	178	27.2	507
	213	20		7.6			15.3	1.84	178	27.3	427
	208	30		7.7			15.5	1.84	180	26.8	433
	416	40		6.6			15.7	1.82	190	26.8	491
A200	226	10	6.2	8.1	14	13.4	12.8	1.78	140	17.0	>1 μm
	222	20		7.4			13.2	1.78	146	16.6	325
	214	30		7.1			13.4	1.78	140	17.0	378
	215	40		7.2			13.3	1.78	145	16.3	339
A300	227	10	6.2	4.8	9	9.2	8.4	1.81	128	87.5	>1 μm
	217	20		4.5			8.5	1.81	129	82.4	346
	248	30		4.9			8.2	1.81	122	86.2	325
	227	40		5.0			8.7	1.81	126	86.6	335

A200 fumed silica. Scattering intensities for 10 (circles), 20 (triangles) 30 (diamonds) and 40 min (squares) of mixing are shown as well as for the corresponding dry particles (butterflies) [29,40]. Table 1 lists detailed characterization (ϕ_v, $d_{v/s}$, D_f, d_g, n and d_l) for these nanocomposites as well as those filled with 6.2 vol% A150 and A300 and 11.7 vol% OX50 along with the precise thickness of the composite sample, d_{BET} and the nominal particle loading.

4.1.1. Nanocomposites filled with less aggregated SiO_2

Fig. 2a shows that at high q (0.01–0.04 $Å^{-1}$), corresponding to small objects (or primary particles), the power law (Porod's law) [46] decays with a slope equal to $P_1 = -4$ which indicates a smooth particle surface [46]. The primary particle size is 41 nm regardless of mixing time and close to that of dry powders and composites of 11.7 vol% OX50, as expected (Table 1). This is a bit lower than the $d_{BET} = 55$ nm as these are two different averages of the distribution [39]. Also reasonable agreement is obtained (Table 1) for the SiO_2 volume fraction ϕ_v calculated from SAXS (6.5–6.7 vol% and 12.7–13.8 vol%) and its nominal values, 6.2 and 11.7 vol%, respectively [47]. This shows the self-consistency of the SAXS inversion [47]. It should be noted that other particle characteristics could not be obtained by SAXS for the dry powders as it was hart to determine the upper limit of their second Guinier regime (G_2). For example, a distinct 3rd Guinier regime was not detected so neither a distinctive dry aggregate ($G_2 \rightarrow d_g$) nor an agglomerate size ($G_3 \rightarrow d_l$) could be obtained although the presence of rather large structures > 1 μm cannot be excluded. This is a drawback for extracting reliable characteristics beyond $d_{v/s}$ of dry powders by SAXS, SANS or USAXS.

Fig. 2a shows that for OX50-filled composites all SAXS spectra overlap regardless of DAC mixing duration indicating that mixing hardly affects the filler particle structure in the composite. As a result, little variation of aggregate D_f is observed (1.74–1.75) that is comparable to $D_f = 1.6 \pm 0.1$ for dry OX50 powder [48] or $D_f = 1.8 \pm 0.2$ in PDMS composites [16] filled with 2.2–8.1 vol% silica. The aggregate size, $d_g = 236$–281 nm, is in agreement with literature [48,49] and varies rather little also with increasing mixing time and increasing concentration indicating no fragmentation or erosion of aggregate particles with increasing mixing or concentration (Table 1). The number of primary particles per aggregate, n, is about 5–6 in all these composites (Table 1). This is not surprising as OX50 silica particles are some of the largest fumed silica particles with the lowest degree of aggregation according to its manufacturer.

Fig. 2a shows also that above the 2nd Guinier regime (G_2) a third one (G_3) is detected, distinctive by a knee-like increase with a power law (Porod's law) decay of −3 which is somewhat less steep than one would have expected (Fig. 2a, Table 1). A slope of −3 instead of −4 indicates that these are agglomerates with a broad distribution [38]. The characteristic agglomerate sizes ($d_l = 2\,R_{g3}$) in these composites were not affected by mixing time, (t_{mix}). These sizes appeared larger than 1 μm (Table 1) at the low OX50 concentration which is at the limit of what can be measured by USAXS. However, an increase in OX50 loading resulted in smaller agglomerates in the order of 494–746 nm (Table 1). Their sizes are consistent with Fig. 1e,f while the broader agglomerate size distribution ($P_3 = -3$) can also be seen in the broad variability of the measured agglomerate sizes (Table 1). Comparison of agglomerate and aggregate sizes shows that an agglomerate consists of only a few (2–5) aggregates.

4.1.2. Nanocomposites filled with most aggregated SiO_2

Fig. 2b shows the scattering spectra of composites containing 6.2 vol% A200 silica particles at increasing mixing duration along with those of dry A200 (butterflies). Here mixing hardly affects the large q tail of the SAXS spectrum indicating little variation in primary particle size ($d_{v/s}$ = 13 nm), aggregate size (d_g = 140–146 nm) and also n = 16–17 (Table 1). The primary particle size is consistent with dry particle SAXS and BET measurements (Table 1) [38] as well as the aggregate size obtained by high pressure expansion of A200 aqueous suspensions [49].

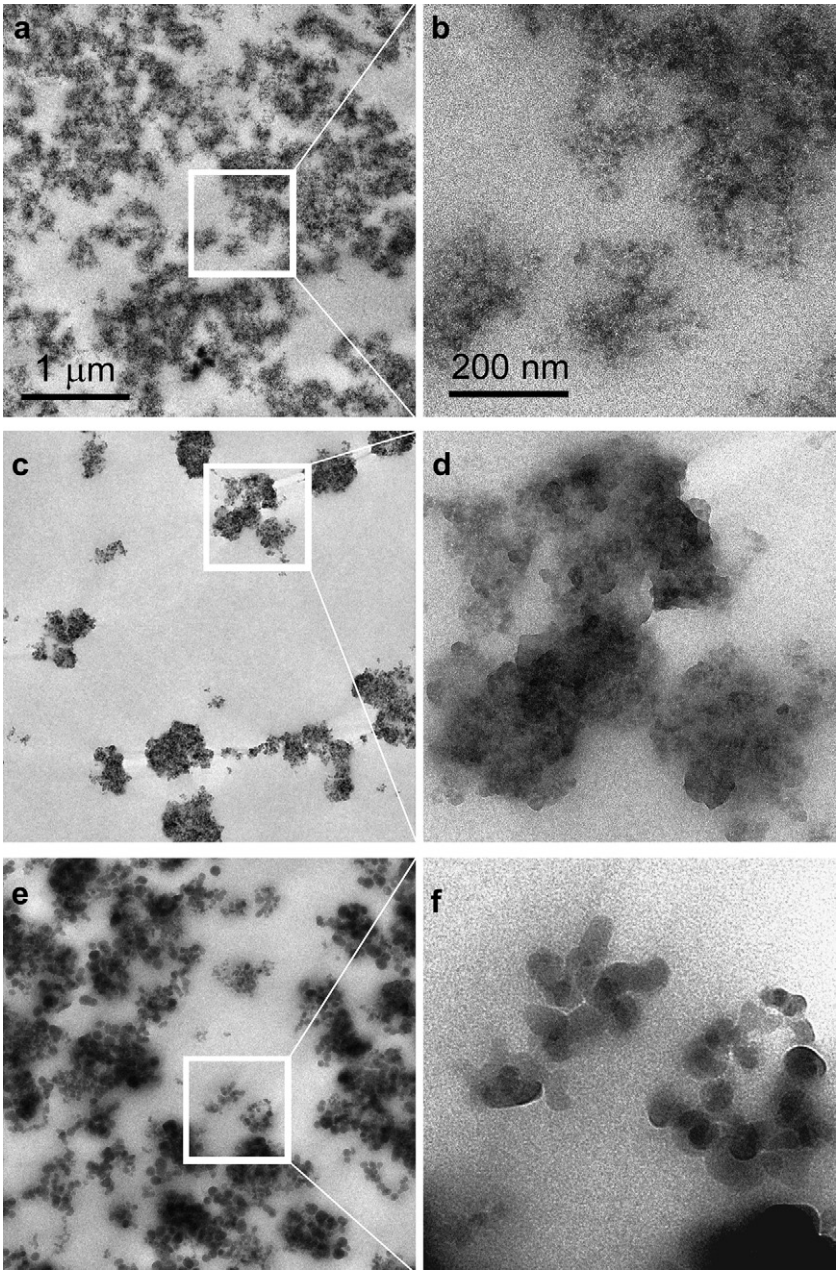

Fig. 1. Images of cryostate-microtome thin-sectioned composites with 6.2 vol% A300 (a–d) and 11.7 vol% OX50 (e,f) filler content mixed for 10 (a,b) or 30 min (c–f). Scale bars are identical for (a,c,e) and (b,d,f).

Since A200 is more aggregated than [49] OX50 as also seen from the higher n, it has a narrower primary particle size distribution [50] that helps to get a better agreement [39] between $d_{v/s}$ and d_{BET}. The D_f (=1.78) is close to that measured for A200 powders [39,48] or A200-filled PDMS [16]. The A200 aggregate size in the composites is not consistent with that of dry A200 particles where huge values ($R_{g2} > 1$ μm) were obtained [39]. This emphasizes that measuring dry particle characteristics by U/SAXS is challenging as seen for OX50 also (Fig. 2a, Table 1), since the close proximity between dry particles hinders the distinction between aggregates and agglomerates. The silica volume fraction $\phi_v = 7.1–8.1$ vol% was slightly larger than for OX50 filled composites but still consistent with the nominal value (6.2 vol%).

While mixing hardly affected the large q tail of the SAXS spectrum (small particles), distinct variations were observed at the small q tail (large particles) especially for the composite with $t_{mix} = 10$ min (circles). The scattering intensity at $q < 0.002$ Å^{-1} did not show the power law slope of −4, but rather one comparable to P_2 (=−1.78) emphasizing the similarity of scattering curves as detected for dry particles [39]. A power law slope less steep than −4 is an indication of a rather broad agglomerate size distribution as detected for OX50 (Fig. 2a) but more pronounced here. After 20 min of mixing, the power law slope P_3 was equal to −4 and the agglomerate sizes were not affected by further mixing and were in the order of d_l = 325–378 nm (Table 1). This emphasizes that sufficient mixing is needed to establish consistent and uniform agglomerate sizes.

In Table 1 composites with 6.2 vol% of A150 and A300 are also listed. Their characteristics as a function of mixing duration were similar to A200 with respect to D_f and their $d_{v/s}$ was consistent with dry powder SAXS and d_{BET} measurements (Table 1). Their n (A150: 27, A300: 82–88), however, were consistently different than for

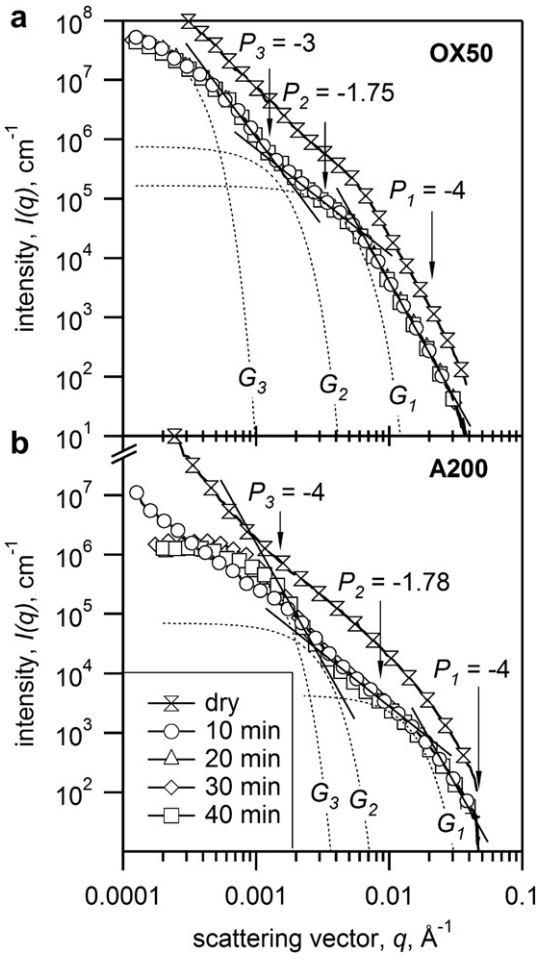

Fig. 2. Combined U/SAXS spectra of dry SiO_2 particles (butterflies) and composites filled with (a) 6.2 vol% OX50 or (b) A200 for varying t_{mix} (10: circle, 20: triangles, 30: diamonds, and 40 min: squares). Unified fit for Guinier (G_1, G_2, G_3, broken lines) and Porod (P_1, P_2, P_3, solid lines) regimes describing the primary particle (*1*), aggregate (*2*) and agglomerate (*3*) characteristics.

A200 due to the difference in $d_{v/s}$ and d_g (A150: 178–190 nm, A300: 122–129 nm). These d_g were consistent with high pressure fragmented A150 and A300 suspensions measured by DLS, d_{DLS} = 210 and 180 nm, respectively [51]. In contrast to the OX50 filled composites, the ones filled with A200 or A300 need mixing for at least 10 min to break up large agglomerates (>1 μm). Resulting agglomerate sizes of the A300 filled composite mixed for 10 and 30 min were consistent with TEM images (Fig. 1a–d): rather large structures in the order of microns for composites mixed in short times and slightly smaller for 30 min mixing. Overall it should be noted that aggregate and primary particle sizes are determined during synthesis of filler particles as the mixing in polymer hardly affects these sizes in every filler of Table 1. Cooling rate, maximum flame temperature and precursor concentration determine such sizes for flame-made titania [52] and silica [53] as employed here.

4.2. Mechanical properties of cured nanocomposites

4.2.1. Crosslinker content

In Fig. 3 the optimum concentration of crosslinker was determined by swelling cured nanocomposites in toluene. The absorbency *A* is decreasing for increasing crosslinker concentration as seen for unfilled polymers (butterflies) and filled ones with 6.2 vol% OX50 (diamonds), A200 (triangles) and A300 (circles). Generally,

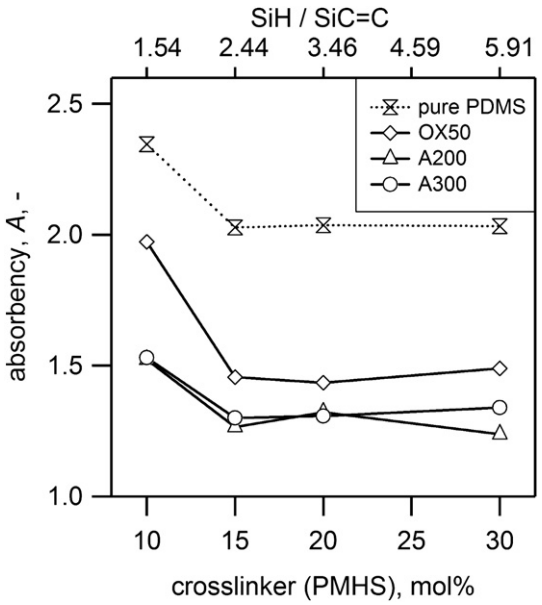

Fig. 3. Absorbency as a function of crosslinker content for particle-free polymer (doted line) or 6.2 vol% filled OX50 (diamonds), A200 (triangles) or A300 (circles) composites mixed for 40 min, swollen in toluene for 24 h and dried for 24 h at 80 °C and 30 mbar. On the top abscissa, the corresponding SiH/SiC=C ratios are shown.

unfilled polymers swelled the most in toluene: at low crosslinker concentrations (10 mol%), the absorbency was 2.3 indicating lower strength [31]. Above 15 mol%, the *A* is invariable with crosslinker concentration indicating that this is the optimum of crosslinker content, in agreement with literature [30] where an optimum of 12.5 mol% was reported by mechanical tensile tests for identical PDMS components. Addition of excess crosslinker does not increase crosslinking density due to saturation.

The ratio of Si–H (from the crosslinker) to Si-vinyl bonds (SiH/SiC=C) for the presented crosslinker/vinyl-terminated PDMS component mixtures were calculated accounting also for the additional SiC=C contribution from the catalyst. The corresponding ratios are listed at the top of Fig. 3 varying from 1.54 (10 mol% PMHS) to 5.91 (30 mol%) which means an excess of crosslinker for all applied concentrations. An optimum ratio is between 1.54 and 2.44 for an unfilled polymer in agreement with suggested ratios [6] of SiH/SiC=C equal to 1.8. Here the applied crosslinker consists of one Si–H bond per Si from the Si–O backbone (approx. 35 Si–H per PMHS molecule). Depending on the number of Si–H bonds per crosslinker molecule and the accessibility for crosslinking, different optimum crosslinker concentrations [6] can be obtained, here.

The addition of 6.2 vol% OX50 did not change the optimum concentration of crosslinker but *A* was reduced considerably below 2. With admixing of A200 or A300 the reduction of *A* was even more pronounced though no significant difference between them was found. The addition of SiO_2 particles to PDMS composites reduces the swelling ability or increases the apparent crosslinking density following the Flory-Rehner rubber swelling theory [32]. Particles with higher *SSA* and more aggregated structures (Table 1) like A200, A300 led to a lower absorbency *A* than OX50. This is driven by the larger available particle surface area and PDMS chain entanglement of adsorbed molecules therefore increasing the crosslinking density [5,6]. More important is that the trend of the unfilled polymer was preserved: an optimum crosslinker concentration of 10–15 mol% for all filler containing (OX50, A200, A300) polymers [6,30]. Moreover it was also reported that –OH present at the SiO_2 particle surface has the ability to chemisorb the crosslinker releasing H_2 as a reaction product [54] which leads to a slight

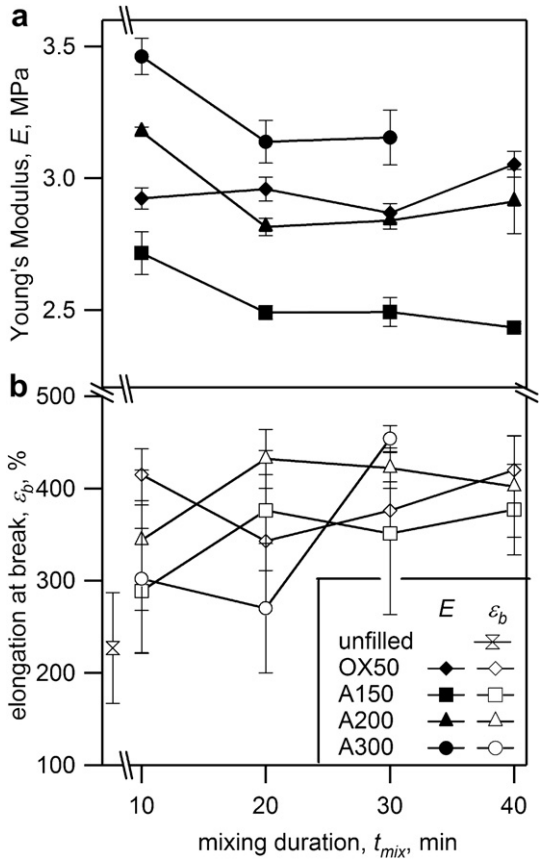

Fig. 4. Tensile measurements of unfilled (butterfly) and filled composites: 11.7 vol% OX50 (diamonds), 6.2 vol% A150 (squares), A200 (triangles) and A300 (circles). (a) Evolution of Young's modulus (E, filled symbols) and (b) elongation at break (ϵ_b, open symbols) as a function of t_{mix}.

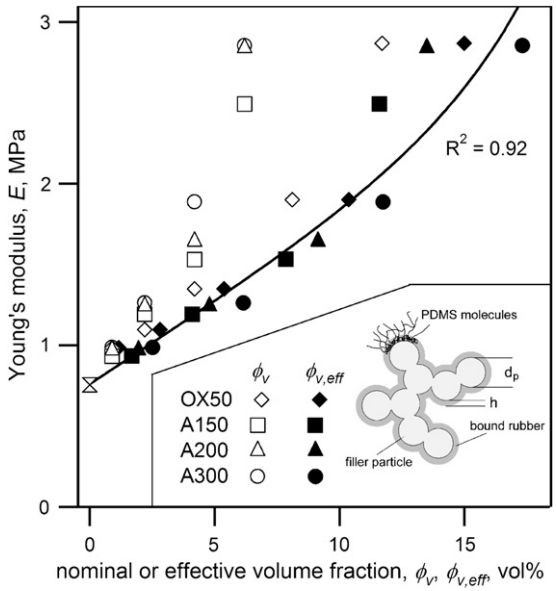

Fig. 5. Reinforcing of SiO_2-filled PDMS composites: Young's modulus E as a function of silica volume fraction ϕ_v (open symbols) or effective volume fraction $\phi_{v,\mathrm{eff}} = \beta \times \phi_v$ (filled symbols) taking into account bound rubber (with inset sketch [44]). For OX50 (diamonds), A150 (triangles) and A200 (circles) t_{mix} was 20–30 min while for A300 t_{mix} = 10–30 min. For the calculation of β from Eq. (1), a bound rubber thickness, h = 2.5 nm, a mean number of adjacent particles or coordination number [45], c_N = 3, and a primary particle size equal to d_{BET} (Table 1) were used.

consumption of Si–H. As a consequence, a crosslinker content of 20 mol% was used for all composites here.

4.2.2. Young's modulus E elongation at break

Fig. 4 shows tensile test measurements of unfilled (butterflies) and filled polymers with 11.7 vol% OX50 (diamonds), 6.2 vol% A150 (squares), A200 (triangles), and A300 (circles) as a function of DAC mixing duration, t_{mix}. Indicated error bars resulted from at least 3 measurements. The Young's modulus E (Fig. 4a, filled symbols) slightly decreases with t_{mix} for composites with more aggregated SiO_2 powders (A150, A200 and A300) while for the less aggregated SiO_2 (OX50) a rather invariant evolution with mixing duration was observed consistent with the agglomerate size of Table 1. So the order of increasing reinforcement is: unfilled < A150 < A200 < OX50 (though higher loading of 11.7 instead of 6.2 vol%) < A300. For 6.2 vol% OX50-filled composites one would expect, however, lower E than for A150 filled PDMS, in the order of E = 1.3–1.9 MPa, as seen from interpolations later on in Fig. 5. For A200 and A300, a mixing duration of at least 20 min was necessary to reach non-varying composite or filler distribution and size properties (Table 1). Comparison of the measured E to literature is difficult as it is known that polymer molecular weight or chain length, particle loading and specific particle characteristics (*SSA*, morphology) affect mechanical reinforcing. However, reported values of a different filler size and content (8.2 vol% A130) in a lower molecular weight monomers [6] results in E = 3.18 MPa and unfilled PDMS composite from similar molecular weight [6,30] resulted in E = 0.58 MPa consistent with E = 2.5 and 0.8 MPa, for the A150-filled composite and unfilled polymer, respectively, here.

Fig. 4b shows also the elongation at break (ϵ_b, open symbols). In general, the error bars depicted are significantly larger than those of E. This makes it more difficult to find distinct trends. Similar to E, also the ϵ_b for OX50-filled composites (diamonds) was within the measurement error indicating that it was not affected by mixing duration. For A150 and A200, however, longer mixing slightly increases ϵ_b but becomes invariable after t_{mix} = 20 min. Both E and ϵ_b evolution as a function of mixing duration are consistent with U/SAXS (Table 1, Fig. 2) and TEM images (Fig. 1a–d) with respect to agglomerate sizes at t_{mix} = 10 min or $t_{mix} \geq$ 20 min or particle dispersion, respectively.

4.2.3. Effect of particle volume fraction

Fig. 5 shows the Young's modulus E of OX50 (diamonds), A150 (squares) A200 (triangles) and A300 (circles) filled composites as a function of particle volume fraction ϕ_v (open symbols). At particle loadings above 2.5 vol% it is seen that A150, A200 and A300 exhibit significantly higher reinforcing ability (larger E) than OX50. However at low particle loading (below 2.5 vol%) the variations between particles are not significant and the evolution of E with decreasing ϕ_v nicely approaches that of unfilled polymers (butterfly), E = 0.8 MPa.

For aggregated particles having a high *SSA*, the reinforcing ability can not only be explained by the particle volume fraction but also by their large available surface area. This was recognized early on for natural rubbers filled with carbon black or silica [1]. The primary particle size, d_p, from Eq. (1) might be best covered by d_{BET} or $d_{v/s}$. However, the morphology of fumed SiO_2 is rather fractal as seen from SAXS where the D_f varies from 1.74 (OX50) to 1.81 (A300) and particles consist of n = 5 (OX50) to 88 (A300) primary particles per aggregate (Table 1). A non-branched chain-like aggregate would exhibit a coordination number c_N = 2 whereas 8 corresponds to cubic body centered structure. Fumed SiO_2 might be in the order

of $2 < c_N < 3.3$ depending on fractal structure [45]. To estimate the extent of variation of the effectiveness factor β by the unknown "bound rubber" thickness h and coordination number c_N of SiO_2 surrounded by PDMS, a minimum β was calculated by applying a minimum $h = 1$ nm and a dense particle morphology $c_N = 3.3$ and a maximum $h = 4$ nm and a chain-like particle morphology ($c_N = 2$). As a result, the calculated β from Eq. (1) was in order of 1.11–1.47 (OX50), 1.34–2.61 (A150), 1.45–3.28 (A200) and 1.68–4.80 (A300). Particles consisting of smaller primary particles (like A150, A200 and A300) have a high specific surface area which tends to bind more rubber, resulting in a larger effective volume, hence larger β. With increasing *SSA* also the extent of uncertainty rises as seen from the calculated range of feasible β factors above.

In Fig. 5 the Young's modulus E is also plotted versus the calculated $\phi_{v,\mathrm{eff}} = \beta \times \phi_v$ (open symbols). The β was calculated assuming for all particles the same $h = 2.5$ nm and $c_N = 3$. This results in the following effectiveness factors: OX50: $\beta = 1.28$, A150: 1.87, A200: 2.17 and A300: 2.79. The chosen coordination number $c_N = 3$ might be smaller for aggregated particles such as A150, A200 or A300. These are consistent, however, with those reported for PDMS of different molecular weight filled with OX50 ($\beta = 1.1$) and A200 ($\beta = 2.7$) [16]. Compared to A300 and OX50 filled natural rubbers [44], these values are smaller but this is explained by the difference in type of polymer [2,9].

Particles consisting of smaller primary particles (hence higher *SSA* and higher extent of aggregation) were shifted towards higher "effective" volume fractions as they tend to trap or capture more polymer. For example $\phi_v = 6.2$ vol% becomes $\phi_{v,\mathrm{eff}} = 17.3$ vol% for A300 while a $\phi_v = 11.7$ vol% becomes only $\phi_{v,\mathrm{eff}} = 15.0$ vol% for OX50. Comparison of filled to open symbols in Fig. 5 shows that indeed a better correlation of mechanical strength to particle loading is found when an additional volume uptake by the bound rubber is included. However, one has to be careful when applying Eq. (1), as the effectiveness factor is strongly affected by the estimation of the "bound rubber" thickness h and to a lesser extent by the coordination number c_N. The line in Fig. 5 was obtained from the rather linear increase at low $\phi_{v,\mathrm{eff}}$ and the additional exponential term for higher $\phi_{v,\mathrm{eff}}$:

$$E\left(\phi_{v,\mathrm{eff}}\right) = 0.755 + 0.1 \times \phi_{v,\mathrm{eff}} + 0.005 \times \exp\left(0.281 \times \phi_{v,\mathrm{eff}}\right) \quad (2)$$

which resulted in $R^2 = 0.92$ with the presented data.

The mechanics of filled composites are determined from the strength of particle–particle and particle-polymer interactions. The applied mechanical load is transferred from the polymer via the interface to the filler. The particle size or the related specific surface area defines the number of adhesive points for potential interaction of polymer and filler, while the particle surface chemistry and choice of polymer defines the strength of filler–polymer interaction. Hence, increasing the potential interaction points by increasing the filler loading or *SSA* (with reduction of primary particle size) enhances the composite reinforcing [55] as shown in Fig. 5.

The morphology of flame-made nanoparticles affects the mechanics of their nanocomposites also. For a given filler mass, aggregated filler particles tend to influence bigger volumes than their equivalent spherical ones. Such fillers consist of several primary particles per aggregate and therefore result in relatively large aggregate sizes. This reduces the amount of filler needed to reach the critical loading where inter-connected aggregates built-up a macro structure (percolation network) throughout the composite, also referred to the gelation point [55]. The effect of aggregates accounts largely for the exponential term in Eq. (2). It should be noted that aggregates of nanoparticles are credited also with enhanced electron conductivity and essentially performance of metal oxide gas sensors [56].

5. Conclusions

Commercially available SiO_2 particles (OX50, A150, A200 and A300) were admixed into PDMS at different concentrations (up to 12 vol%) with a planetary mixer (dual asymmetric centrifuge). Low *SSA* particles with limited aggregation like OX50 were processed comfortably up to 11.7 vol%. In contrast, particles with higher *SSA* and rather aggregated morphology (like A200 or A300) can be processed to 6.2 vol% content. The reinforcing capacity of such fillers increases significantly the polymer viscosity.

No variation of aggregate sizes and mass fractal dimension of the filler particles in these composites with mixing duration was observed by U/SAXS, as expected. The measured filler loadings and primary particles in the composites were consistent also with the nominal values applied pointing out the reliability of the U/SAXS measurements. The less aggregated morphology of OX50 revealed ($n = 5$–6) few primary particles per aggregate in contrast to the more aggregated powders of A150, A200 or A300 that had n ranging from 16 to nearly 90. Only changes of the agglomerate sizes with increasing mixing duration were detected indicating that sufficient mixing is needed to establish consistent and uniform agglomerate sizes in the composites. More aggregated fillers or powders needed longer mixing than less aggregated ones. Moreover, the method of particle admixing into PDMS showed the limitations of the widely used "scotch tape" method (in U/SAXS) for measuring the aggregate and agglomerate sizes of such dry powders or fillers.

Agglomerate size visualization with TEM imaging of thin composite sections cut with a cryostate-microtome were consistent with X-ray scattering results while U/SAXS analysis clearly demonstrated the capacity to distinguish between aggregates and agglomerates, a known shortcoming of the rather subjective evaluation of TEM images.

An optimum crosslinker amount for unfilled and filled composite was found by swelling composites in toluene at a SiH/SiC=C ratio between 1.54 and 2.44 consistent with literature. The reinforcing capacity of SiO_2 fillers (stronger for A200, A300 than OX50) was observed from their increased crosslinking density or reduced toluene absorbency. Prolonged mixing duration resulted in reduced Young's modulus and increased elongation at break, most probably a result of agglomerate size reduction (as seen from U/SAXS) and changes in particle dispersion (from TEM).

The model of increased volume fraction (the so-called effective volume fraction) by the uptake of "bound rubber" (immobilized polymer layer adsorbed at the particle surface) described the effect of filler reinforcement on the mechanical properties of the composites. The reinforcing capacity of several types of SiO_2 filler can be described by a single expression as function of effective volume fraction rather than the sole, solid SiO_2 volume fraction. So filler-induced reinforcing of PDMS-based composites is driven by the *SSA* and extent of aggregation of such fumed SiO_2 fillers.

Acknowledgements

Molding of composites was performed with equipment designed and provided by PFISTERER SEFAG AG. We thank L. Diener and Dr. R. Wepf at EMEZ (ETH Zurich) for ability to use the cryostate-microtome thin sectioning, Dr. F. Krumeich (EMEZ) for TEM imaging, K. Feldman at D-MATL (ETH Zurich) for use of the tensile test equipment. The use of the ESRF beam line ID02

(Grenoble) for SAXS measurements was possible through the support of the experiment MA-564. Financial support from Swiss National Science Foundation (SNF 200021-114095) and Commission of Technology and Innovation (CTI-7949.3) are acknowledged.

References

[1] Kraus G. Rubber Chem Technol 1978;51(2):297–321.
[2] Shim SE, Isayev AI. Rheol Acta 2004;43(2):127–36.
[3] Clement F, Bokobza L, Monnerie L. Rubber Chem Technol 2005;78(2):211–31.
[4] Barna E, Bommer B, Kursteiner J, Vital A, von Trzebiatowski O, Koch W, et al. Compos Part A-Appl 2005;36(4):473–80.
[5] Aranguren MI, Mora E, Degroot JV, Macosko CW. J Rheol 1992;36(6):1165–82.
[6] Aranguren MI, Mora E, Macosko CW, Saam J. Rubber Chem Technol 1994;67 (5):820–33.
[7] Paquien JN, Galy J, Gerard JF, Pouchelon A. Colloid Surf A 2005;260(1–3):165–72.
[8] Litvinov VM, Barthel H, Weis J. Macromolecules 2002;35(11):4356–64.
[9] Aranguren MI, Mora E, Macosko CW. J Colloid Interf Sci 1997;195(2):329–37.
[10] Demir MM, Menceloglu YZ, Erman B. Macromol Chem Physic 2006;207 (16):1515–24.
[11] Wen JA, Mark JE. J Appl Polym Sci 1995;58(7):1135–45.
[12] Ulrich GD. Chem Eng News 1984;62(32):22–9.
[13] Strobel R, Pratsinis SE. J Mater Chem 2007;17(45):4743–56.
[14] Schulz H, Schimmoeller B, Pratsinis SE, Salz U, Bock T. J Dent 2008;36(8):579–87.
[15] Todd DB, editor. Mixing of highly viscous media. Weinheim: Wiley-VCH; 2004.
[16] Piau JM, Dorget M, Palierne JF. J Rheol 1999;43(2):305–14.
[17] Dreiss CA, Cosgrove T, Benton NJ, Kilburn D, Alam MA, Schmidt RG, et al. Polymer 2007;48(15):4419–28.
[18] Charles S.B, Kinney R.J, Kropp M.A, Mader R.A. No-flow flux adhesive compositions in U.S. Patent No. 6528169; 2003.
[19] Bialek A.I, Hill R.M, Kadlec D.A, Van Dort H.M. Temperature insentive one-phase microemulsions in U.S. Patent No. 6498197; 2002.
[20] Suzuki T, Toth S. Coated silicone rubber article and method of preparing same in U.S. Patent No. 6733893; 2004.
[21] Ziche W, Schindler W. Preparation of organylsilyl-terminated polymers in U.S. Patent No. 7319128; 2008.
[22] Frances J.M. Dental composition based on a functionalized silicone crosslinkable and/or plymerizable by heat-process in U.S. Patents No. 7129282; 2001.
[23] Huang M, Kropp M.A. Photocurable form-in-place gasket for electronic applications in U.S. Patent No. 6670017; 2003.
[24] Block E.J. Sterically hindered reagents for use in single component siloxane cure systems in U.S. Patent No. 7211637; 2007.
[25] Hatcher DW, Preston KR. Cereal Chem 2004;81(3):303–7.
[26] Jacobs O, Xu W, Schadel B, Wu W. Tribol Lett 2006;23(1):65–75.
[27] Choi SB, Jepperson J, Jarabek L, Thomas J, Chisholm B, Boudjouk P. Macromol Symp 2007;249:660–7.
[28] Medalia AI. Rubber Chem Technol 1978;51(3):437–523.
[29] Camenzind A, Schulz H, Teleki A, Beaucage G, Narayanan T, Pratsinis SE. Eur J Inorg Chem; 2008:911–8.
[30] Osman MA, Atallah A, Muller M, Suter UW. Polymer 2001;42(15):6545–56.
[31] Vera-Graziano R, Hernandez-Sanchez F, Cauich-Rodriguez JV. J Appl Polym Sci 1995;55(9):1317–27.
[32] Flory PJ, Rehner J. J Chem Phys 1943;11(11):521–6.
[33] Freeman HA, Durall RL, editors. Microscopical characterization. New York: John Wiley & Sons; 1991.
[34] Narayanan T, Diat O, Bosecke P. Nucl Instrum Meth A 2001;467:1005–9.
[35] Sztucki M, Gorini J, Vassalli JP, Goirand L, van Vaerenbergh P, Narayanan T. J Synch Rad 2008;15:341–9.
[36] Sztucki M, Narayanan T. J Appl Crystallogr 2007;40:S459–62.
[37] Beaucage G. J Appl Crystallogr 1995;28:717–28.
[38] Beaucage G, Kammler HK, Pratsinis SE. J Appl Crystallogr 2004;37:523–35.
[39] Kammler HK, Beaucage G, Mueller R, Pratsinis SE. Langmuir 2004;20 (5):1915–21.
[40] Hyeon-Lee J, Beaucage G, Pratsinis SE, Vemury S. Langmuir 1998;14(20):5751–6.
[41] Einstein A. Ann Phys-Leipzig 1906;19(2):289–306.
[42] Guth E. J Appl Phys 1945;16(1):20–5.
[43] Thomas DG. J Coll Sci Imp U Tok 1965;20(3):267–77.
[44] Eggers H, Schummer P. Rubber Chem Technol 1996;69(2):253–65.
[45] Friedlander SK. Smoke, dust and haze: fundamentals of aerosol dynamics. New York: Oxford University Press; 2000.
[46] Porod G. In: Glatter O, Kratky O, editors. Small-angle x-ray scattering. London: Academic Press; 1982.
[47] Kammler HK, Beaucage G, Kohls DJ, Agashe N, Ilavsky J. J Appl Phys 2005;97(5).
[48] Mueller R, Kammler HK, Pratsinis SE, Vital A, Beaucage G, Burtscher P. Powder Technol. 2004;140(1–2):40–8.
[49] Wengeler R, Teleki A, Vetter M, Pratsinis SE, Nirschl H. Langmuir 2006;22 (11):4928–35.
[50] Heine MC, Pratsinis SE. J Aerosol Sci. 2007;38(1):17–38.
[51] Wengeler R, Nirschl H. J Colloid Interf Sci 2007;306(2):262–73.
[52] Heine MC, Pratsinis SE. Part PArt Syst Charact 2007;24(1):56–65.
[53] Tsantilis S, Pratsinis SE. Langmuir 2004;20(14):5933–9.
[54] Reihs K, Colom RA, Gleditzsch S, Deimel M, Hagenhoff B, Benninghoven A. Appl Surf Sci 1995;84(1):107–18.
[55] Camenzind A, Caseri WR, Pratsinis SE. Nano Today 2010;5(1):48–65.
[56] Keskinen H, Tricoli A, Marjamaki M, Makela JM, Pratsinis SE. J Appl Phys 2009;106(8):084316.